Self-sensing concrete made from recycled carbon fibres

I. Segura[a,b,*], G. Faneca[d], J. M. Torrents[c], A. Aguado[b]

[a] Smart Engineering Ltd., C/Jordi Girona 1-3, Parc UPC – K2M, 08034, Barcelona, Spain

[b] Department of Civil and Environmental Engineering, Universitat Politècnica de Catalunya - Barcelona Tech, C1, 08034, Barcelona, Spain

[c] Department of Electronics Engineering, Universitat Politècnica de Catalunya - Barcelona Tech, C4, 08034, Barcelona, Spain

[d] Escofet 1886 Ltd. 08760 Martorell Barcelona

Abstract

The electrical and piezo-resistive responses of recycled carbon fibre (rCF)-reinforced concrete is analysed in this article. Two different PAN-based rCFs (monofilament rCF and fibrillated rCF sheets) incorporated into dry concrete mix were investigated. Piezo-resistivity was evaluated by simultaneously monitoring the variation in the applied DC voltage during both flexural and compressive tests. Although both plain and rCF-reinforced concrete samples showed piezo-resistive responses, the latter show increased signal-to-noise-ratio and thus behave like self-sensing materials. The electrical behaviour suggests a mixed control owing to both ionic and electronic conductivity, with the dominant one depending on the rCF content

* Corresponding author: Ignacio Segura Pérez. Universitat Politecnica de Catalunya. Departament d'Enginyeria de la Construcció. Carrer Jordi Girona 1-3, Edifico C1, despacho 202. E-08034 Barcelona. SPAIN. Email: ignacio.segura@upc.edu. Tel.: +34-93-401-65-30. Fax: +34-93-405-41-35

and rCF dispersion. This work enhances the possibility of generalising the use of smart cementitious materials in the civil engineering industry.

Keywords

Self-sensing concrete; strain sensing; recycled carbon fibre; smart material

1. INTRODUCTION

Since the last 15 years, there is a revolution to turn civil infrastructures and buildings all over the world into smart structures. Our current society is increasingly demanding that the infrastructures and cities become smart and provide other functionalities in addition to their mechanical performance and durability. Furthermore, the recent failures in the summer of 2018 of a motorway bridge in Genova, Italy and of a concrete pier in Vigo, Spain, have brought the focus on how our society deals with infrastructure monitoring and maintenance. Moreover, there is a need to reduce monitoring costs and to avoid further collapse of existing infrastructures.

This revolution has mainly considered the incorporation of multi-functional devices and sensors into civil infrastructures and architectural heritage. Nowadays, optical fibres are widely employed for monitoring civil infrastructures [1], and wireless sensor networks (WSN) are being extensively used to help preserve the building heritage [2]. One of the main challenges of this approach is the durability of the sensors since they may become *external agents* in the structures. Experience reminds us of the lack of durability of such sensors, as evidenced by dam auscultation and WSN systems. The inconvenient truth is that almost 70% of the sensors fail or are inoperative after 1 year of operation [3]. To describe this situation in medical terminology, we are facing a serious problem of "*transplant rejection"* by our infrastructures.

However, a very promising alternative to the use of conventional sensors is the development of smart cementitious materials with self-sensing abilities, which would allow detection of strain and damages in new and existing infrastructures. The incorporation of conductive phases into cementitious matrices has been one of the most popular methodologies to develop self-sensing cementitious materials. In 1993, Chen and Chung first reported the piezo-resistive effects of carbon fibre-reinforced cementitious materials [4]. The incorporation of conductive phases into the cementitious matrix modifies its conductive characteristic. Thus, piezo-resistive effect appears when stress is applied to the material, owing to the modification of the conductive characteristics of the material. For carbon fibre-reinforced composites, piezo-resistivity is considered to originate from the slight pull-out of crack-bridging fibres during crack opening and the consequent increase in the contact electrical resistivity of the fibre–matrix interface [5], or the conduction network degeneration resulting from fibre reorientation under finite strain [6].

The piezo-resistivity of carbon fibre cementitious materials has been extensively investigated until now [7–12], and nowadays, it is being explored through the incorporation of graphene [13], carbon nanotubes (CNTs) and nanofibers [11,14–17], multiphasic mixes of conductive additives [18–21], and CNT-coated aggregates [22]. An interesting review on the development of self-sensing cementitious materials was published by Chan et al. [23]. However, the incorporation of smart materials into novel or existing infrastructures has not taken off, and has been limited to some pilot studies only [8,17,24,25]. One key reason for this situation is the high cost of the conductive phases that are being used in the development of smart cementitious materials. The use of recycled carbon fibres (rCF) is a very promising alternative in the development of sustainable smart cementitious materials. Recycled carbon fibres are mainly

obtained from aerospace composite scrap. Among many different methods, most of the commercially available rCF are obtained via pyrolysis. This process allow a high retention (up to 90%) of the properties exhibited by virgin carbon fibres [26, 27]. The use of rCF may allow to design economically affordable smart cementitious materials since most of recycling processes yield rCF with high retention of mechanical properties [26] but with a 30 to 40 percent cost savings versus virgin carbon fibre (cost of commercial chopped carbon fibres: 15 €/kg vs cost of rCF: 7-8 €/kg). In a recent paper [28], we demonstrated the possibility of using recycled carbon fibres to develop conductive cementitious materials, and realized electrical resistivities in the range of 3–0.6 Ω·m for rCF contents ranging from 0.2 to 0.8% in vol.

As a continuation of this research, in this study, we explore the capability of recycled fibre cementitious composites as smart materials for self-sensing applications. Two different types of rCF (fibrillated and sheet-type) were evaluated as additives; these two were incorporated at different contents (0.1 to 1.4% in volume) in ultra-high-performance concrete (UHPC) mix. Piezo-resistivity of the prepared concrete samples was evaluated under both flexural and compressive conditions, by taking into account the effect of the moisture content of the samples.

2. MATERIALS AND METHODS

2.1 Concrete dosage and raw materials

The concrete dosage used in our study is shown in **Table 1**; this is characteristic of a UHPC dosage. This concrete dosage was selected because it is expected to enhance the electrical conductivity owing to the presence of a double percolation phenomenon, as described by Wen et al. [5]. The cement selected to produce the UHPC mixtures was a CEM I 53.5R. The sand used was siliceous sand and fine calcium carbonate powder (Betoflow) was incorporated into the different dosages to achieve an optimum workability of the mixes with a low consumption

of superplasticisers. Both a polycarboxylate superplasticiser (Glenium ACE425) and nanosilica suspension (Meyco MS685) were used as additives to provide self-compacting characteristics to the concrete mix. The water to cement (w/c) ratio of the concrete mixes was 0.14. Two different PAN-based rCF samples provided by ELG Carbon Fibre Ltd (C10/30, and CT12) were used in this study. The characteristics of the rCF are described in **Table 2**; C10/30 are monofilament rCF and CT12 are fibrillated sheets of rCF. The fibre factor F given by Eq. 1, as proposed by Narayanan and Darwish, allows to account for the effect of both the geometrical characteristics of the fibres, length (L_f) and diameter (d_f) [29].

$$F = \beta \cdot L_f / d_f \qquad \text{(Eq. 1)}$$

where, β is the fibre shape factor (0.50 for circular fibres), and the fibre was dosage varied from 0.1% to 1.4% in volume.

Table 1. Concrete dosage used for the mixes

Component		**Dosage (kg/m^3)**
Cement		800
Betoflow		220
Sand (0-3/0-1 mm)		1161
Additives	Glenium ACE425	30
	Meyco MS685	57
Water		110

Table 2. Properties of recycled carbon fibres

Property	Value	
	C10/30	**CT12**
Diameter (μm)	7.5	7†
Nominal length (mm)	10–30	12
Average length (mm)	20	12
Fibre factor *F*	1428	12
Density (kg/m^3)	1800	1760
Tensile strength (MPa)	3150	4150
Young modulus (GPa)	200	252
Electrical resistivity (Ω·m)	0.103/0.34††	0.016

† The effective diameter of the fibrillated sheets is 500 μm.
†† The electrical resistivity value varies depending on whether the measurement is made lengthways (0.103) or along the cross-section (0.34)

2.2 Sample fabrication

UHPC samples with dimensions of 40 × 40 ×160 mm were fabricated with the dosages indicated in **Table 1**, according to UNE-EN 196-1 [30]. The concrete samples were produced at the industrial installations of the company, Escofet 1886, with a fabrication procedure replicating the industrial process as closely as possible. Two sets of samples were fabricated from each mix, one set for mechanical measurements and another for electrical measurements. In this work, rCFs were added to the dry mix (D) after incorporating the cement and aggregates. No specific dispersion procedure was implemented since our main aim was to work as close as possible to the real practice and use the actual concrete compositions used in the precast concrete industry. Reference samples were prepared without adding rCF. The electrodes for the electrical measurements were stainless steel set screws of 5 cm length that were introduced 3.5 cm deep into the concrete samples. The samples were cured in a humid chamber (20° ± 2 °C; relative humidity of 95 ± 5%) for 28 days. The samples are designated according to the following code: U-Cf-f-M

where, U stands for UHPC mixes, C_f indicates the fibre content (which varies from 0 for the reference sample to 14 for the 1.4% fibre content), f indicates the fibre type, and M indicates the mixing method of the fibres (D).

2.3 Characterisation

Slump flow was measured according to UNE-EN 1015-3 [31] prior to the development of the concrete samples. Flexural and compressive strength measurements were performed on the concrete samples in compliance with UNE-EN 196-1 [30]; three and six replicates were made for each dosage, respectively. The electrodes used for the electrical measurements were stainless steel set screws of length 5 cm, which were dipped 3.5 cm into the concrete samples. The samples for mechanical strength measurements did not included steel electrodes. Figure 1 shows a scheme on the electrodes positioning on the specimens.

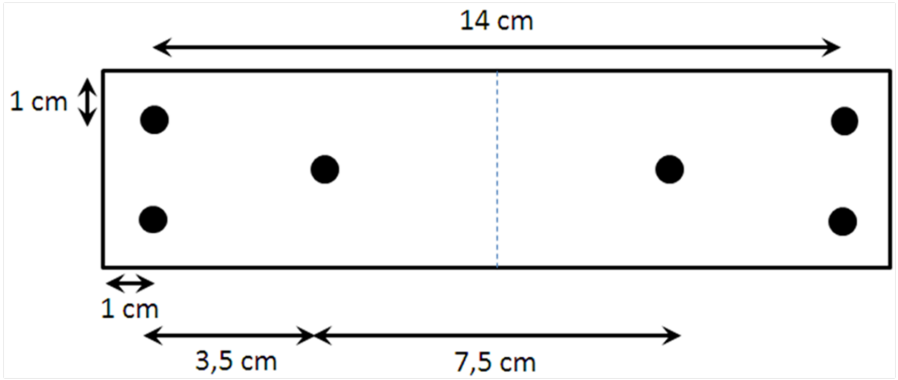

Figure 1. Location of the electrodes in the specimens

The electrical properties of the samples were characterized with an Agilent HP 4192A impedance analyser, using an instrumentation amplifier as a front-end to allow 4-probe measurements [32], with an effective voltage of 1 V AC to avoid polarisation effects in the electrodes [31,32]. The measurements were conducted in the frequency scanning range of 10 Hz to 1 MHz providing electrical impedance (Z, in Ω) and phase (ϕ, in degrees). The

electrical impedance is described by equation 2 and is composed of a real part (resistance, R) and an imaginary part (reactance, X); R and X are given by Equation 3 and 4:

$$Z = R + j \cdot X \quad \text{(Eq. 2)}$$

$$R = Z \cdot \cos\left(\frac{\phi \cdot \pi}{180}\right) \quad \text{(Eq. 3)}$$

$$X = Z \cdot \sin\left(\frac{\phi \cdot \pi}{180}\right) \quad \text{(Eq. 4)}$$

The electrical resistivity (ρ, in Ω·m) was calculated from the impedance data using Eq. 5, where, S is the effective transverse section (0.0016 m^2 in our study), and l is the measurement length (0.07 m in our study). All the samples were allowed to reach a hygrothermic equilibrium by storing them under laboratory conditions for 15 days after finishing the curing period. Lastly, the electrical conductivity (σ, S/m) of the samples was easily calculated as the inverse of the resistivity, using Eq. 6. The electrical conductivity values are expressed as the mean of values determined for three different specimens.

$$\rho = R\frac{S}{l} \quad \text{(Eq. 5)}$$

$$\sigma = \frac{1}{\rho} \quad \text{(Eq. 6)}$$

Piezo-resistivity tests were performed on 40×40×160 mm specimens to evaluate the characteristics of the different conductive concrete samples. Samples were loaded both under flexural and compression conditions. Electric current was passed through the samples using an external DC current source (Keithley Model 6020) to monitor the resistivity variation during the mechanical tests, by fixing the output current to 3 V. Piezo-resistivity measurements were performed on one specimen of each dosage.

3. RESULTS

3.1 Physical and mechanical properties

The influence of the rCF type and content, as well as the mixing method on the slump flow is depicted in Figure 1a. The rCF fibres supplied as fibrillated sheets (CT12) exhibited a larger slump flow compared to that of monofilament rCF (C10/30) at all fibre dosages. A larger slump flow is usually related with better dispersion of the rCF in the cementitious matrix and is strongly affected by the geometrical parameters of the fibre (fibre factor, *F*).

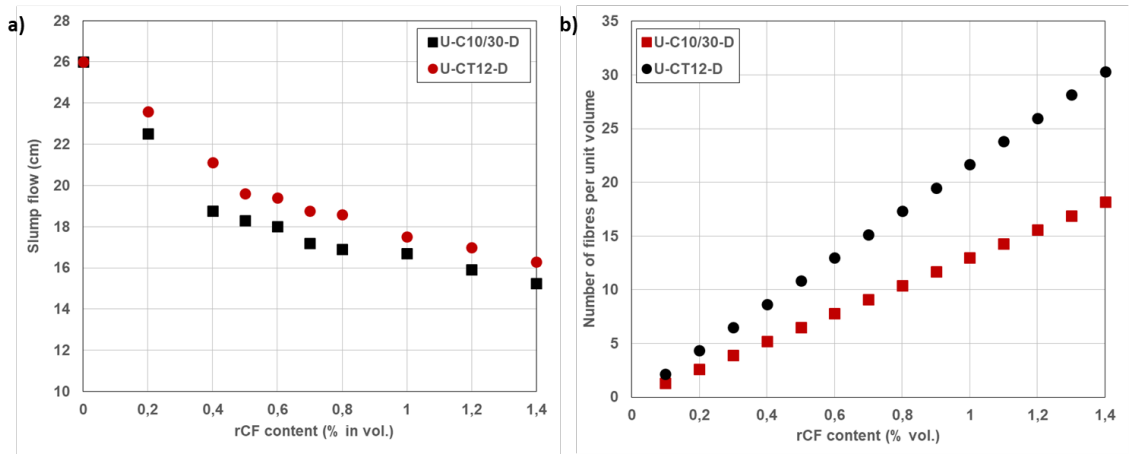

Figure 2. Variation of: (a) slump flow with the content of rCF for the different mixes, and (b) *N* per unit volume with the rCF content for C10/30 and CT12 fibres

Considering the differences in the properties of the two types of rCF shown in **Table 2**, larger differences would be expected in the slump flow of concrete with C10/30 and CT12 samples. However, the fibre dispersion in cementitious materials is affected not only by the fibre factor but also by the number of fibres per unit volume, *N*. This parameter can be calculated according to Eq. 7,

$$N = \frac{V_f}{\pi \cdot \left(d_f/2\right)^2 \cdot L_f} \qquad \text{(Eq. 7)}$$

196 where, V_f is the volume fraction, d_f is the diameter (in mm), and L_f is the length of carbon fibres
197 (in mm). Figure 1b shows the variation of N with the rCF content for concrete samples
198 containing C10/30 and CT12. For low rCF contents, the number of fibres per unit volume is
199 very similar for both samples. As the rCF content increases, the difference between the N values
200 of C10/30 and CT12 samples increases. Thus, the results of slum flow reflect this relationship
201 between the geometrical factor of the fibres and the number of fibres per unit volume.
202
203 The mechanical properties of the specimens shown in Figure 3 also reflect the relationship
204 between the geometrical factor of the fibres and the number of fibres per unit volume.
205 Considering the slump test results shown in Figure 2, a larger mechanical response of CT12
206 samples is expected. However, an inverse trend is observed with the C10/30 specimens
207 exhibiting a larger mechanical response both under compressive and flexural conditions. This
208 result might be explained again in view of the number of fibres per unit volume (N). More
209 carbon fibres in the bulk matrix can result in better mechanical performance up to a certain rCF
210 content given by the fibre factor. Once this value is reached, a further increase in the carbon
211 fibre content might have a weakening effect owing to the presence of air voids and low
212 dispersion of the carbon fibres. As shown in Figure 3a, C10/30 and CT12 samples exhibit
213 almost similar compressive strengths at a low rCF content, because the number of fibres per
214 unit volume is very similar. As the rCF content increases, the difference between the N value
215 of C10/30 and CT12 increases, and thus more defects (air voids and bundles of carbon fibres)
216 might be present in the cementitious matrix.
217

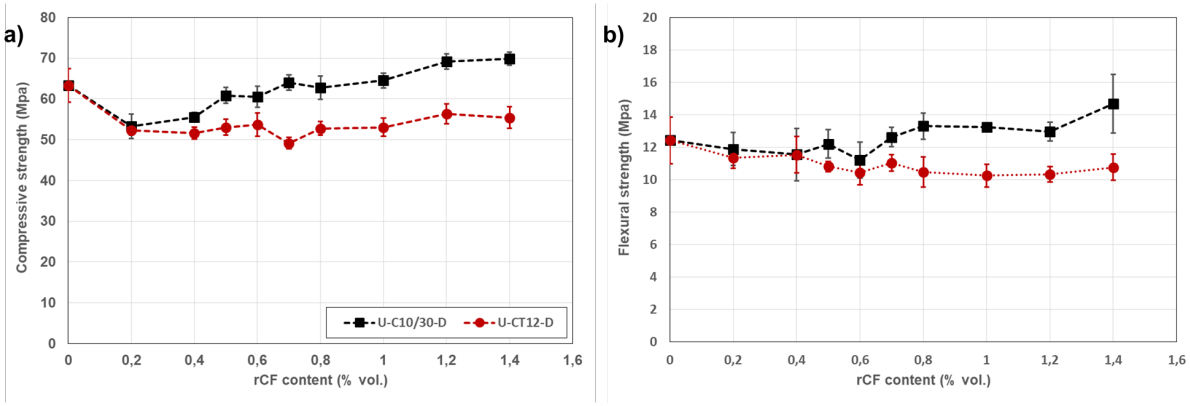

Figure 3. Variation of the a) compressive and b) flexural strengths with the fibre content for different concrete mixes.

3.2 Electrical conductivity

The electrical characteristics of carbon fibre-reinforced cementitious composites are strongly influenced by the applied frequency in AC measurements. Figure 4 shows the Bode diagrams of a reference sample and a sample containing rCF. The reference sample behaves like an insulator with almost no variation in the impedance with the frequency. The incorporation of the rCF modifies the electrical behaviour of the samples, and the impedance reduces as the frequency of the applied current is increased. As stated by several researchers, there is a cut-off frequency that permits bypassing of the cementitious matrix that surrounds the fibres in carbon fibre-reinforced materials [35], referred to as *cusp frequency*. This cut-off frequency is also displayed when rCF is used [28], and the values are 100 and 190 kHz, respectively, for C10/30 and CT12 samples. The electrical resistivities were determined at two different frequency values: 50 Hz and 190 kHz. The first value coincides with the standard frequency for AC, and the second was selected to perform the measurements above the capacitance threshold (C_t) value, and thus bypass the cementitious matrix that surrounds the rCF [26,33].

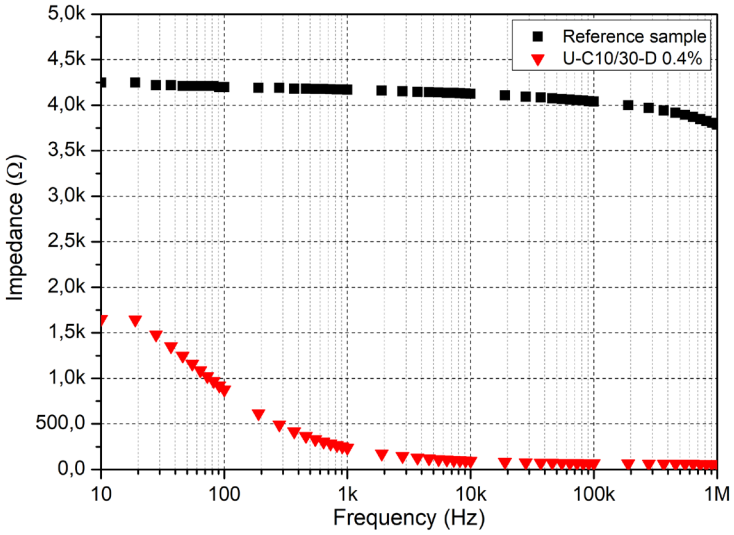

Figure 4. Bode diagrams for a reference concrete sample and an rCF-reinforced sample

The variation of the electrical conductivity with the fibre content for specimens with C10/30 and CT12 is shown in Figure 5, where the y axis presents different limits to accommodate the different limits of both σ_{50Hz} and σ_{190kHz}. For low frequencies (see Figure 5a), specimens with C10/30 exhibit larger electrical conductivity and CT12 specimens present electrical conductivities that are quite similar to that of the reference sample without rCF. Furthermore, the electrical conductivity of samples with C10/30 decreases for fibre contents larger than 0.6% vol. This electrical behaviour is related to the presence of carbon fibre bunches in the cementitious matrix [25]. However, when the capacitance threshold is surpassed (Figure 5b), the electrical behaviour is modified. Whereas the electrical conductivity of the reference sample remains almost invariant (it varies from 0.0178 S/m at 50 Hz to 0.0185 at 190 kHz), there is a strong increase in the electrical conductivity of the specimens containing rCF. The samples with C10/30 fibres present a seven-fold increase in the electrical conductivity on average, while the samples with CT12 fibres show a nineteen-fold increase on average. Although the number of fibres per unit volume of CT12 samples is larger than that of C10/30 samples, the presence of fibre bunches limits the electrical properties of the former. However, for frequencies above the

capacitance threshold, the effect of the fibre bunches on the electrical conductivity is diminished and the electrical conductivity of both C10/30 and CT12 samples becomes equal.

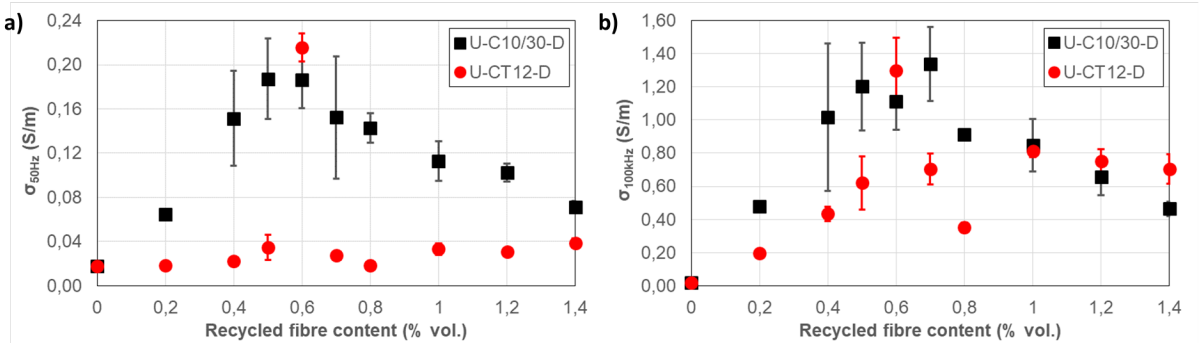

Figure 5. Variation of the electrical conductivity with the fibre content: a) at 50 Hz, and b) at 190 kHz.

The electrical properties of carbon fibre-reinforced cementitious composites depend mostly on two different parameters: the dispersion of the fibre in the cementitious matrix and the waviness of the carbon fibres. The goodness of fibre dispersion in the cementitious matrix will determine the presence of fibre agglomerates (clusters). Furthermore, the characteristics of the carbon fibres usually utilised in cementitious composites may affect its waviness and thus its actual length. Both parameters will determine the presence of a continuous path of fibres and thus the electrical conductivity of the composite. García-Macías [36] studied both the effect of clustering and waviness on the electrical conductivity of CNT cementitious composites. The results shown in Figure 5 are consistent with the combined effect of clustering and waviness.

3.3 Piezo-resistive response of specimens under laboratory conditions

Figure 6 shows the load-voltage curves obtained for different concrete specimens made with different contents of C10/30 rCF during compression tests. First, it is noticeable that the reference specimen without rCF also shows a piezo-resistive effect. A small variation in the

voltage curve can be observed repeatedly, coinciding with the maximum and minimum values of the applied load. The piezo-resistive responses were also observed using DC, and thus ionic effects can be observed in the voltage curve represented by the voltage drop from the start to the end of the test.

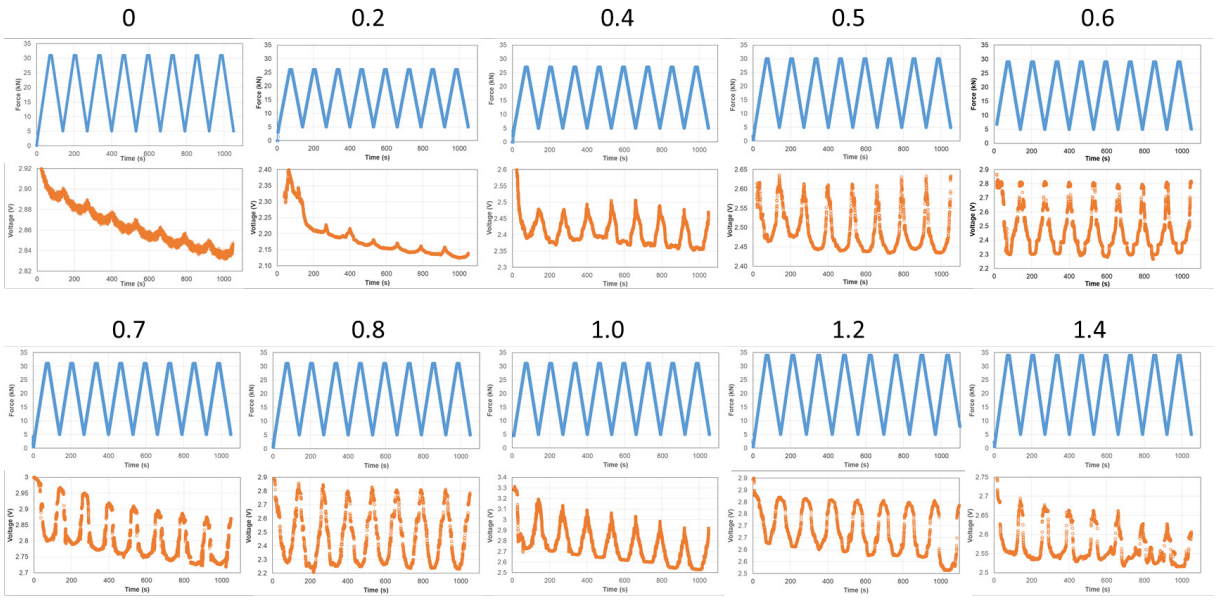

Figure 6. Load-voltage curves for the concrete specimens prepared with C10/30 rCF during the compression tests. The numbers above the curves indicate the rCF content of the concrete specimens.

The introduction of the rCF has a remarkable effect on the voltage curve; it increases the amplitude of the voltage variation. The amplitude of the voltage variation depends on the rCF content and increases up to a fibre content of 0.8%. However, the introduction of rCF also affects the stability of the voltage curve and for fibre contents above 0.2%, the initial and final voltage is almost the same for different specimens. No evidences of the piezo-resistive effect were observed upon analysing the load-voltage curves obtained from flexural tests (see Figure 7).

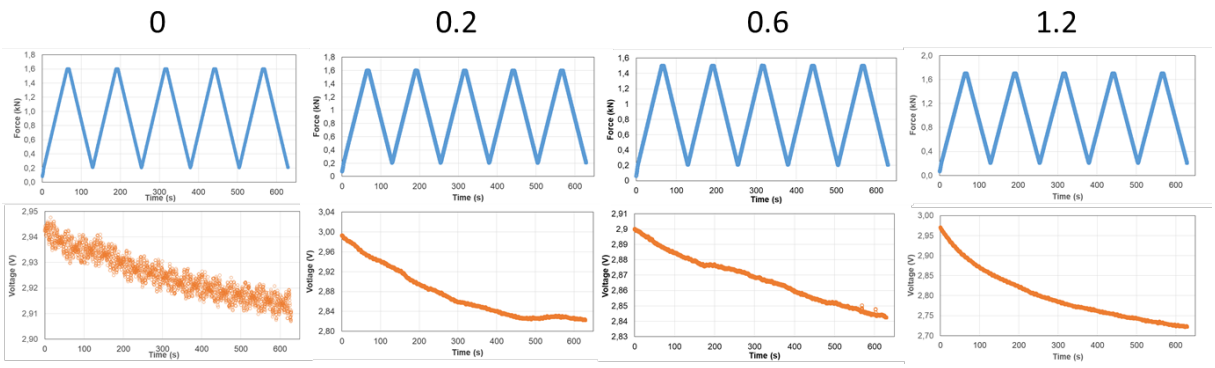

Figure 7. Load-voltage curves for the concrete specimens containing C10/30 rCF during the compression tests. The numbers above the curves indicate the rCF content of the concrete specimens.

Similar load-voltage curves were obtained for the specimens containing CT12 fibres, indicating a piezo-resistive phenomenon during the compression tests (see Figure 8), but no clear evidence of it was found during the flexural tests. The load-voltage curves in Figure 8 present some distinctive features presenting more noise and more irregular patterns that those shown in Figure 6. The different data obtained from the load-voltage curves during the compression tests are collected in Table 3.

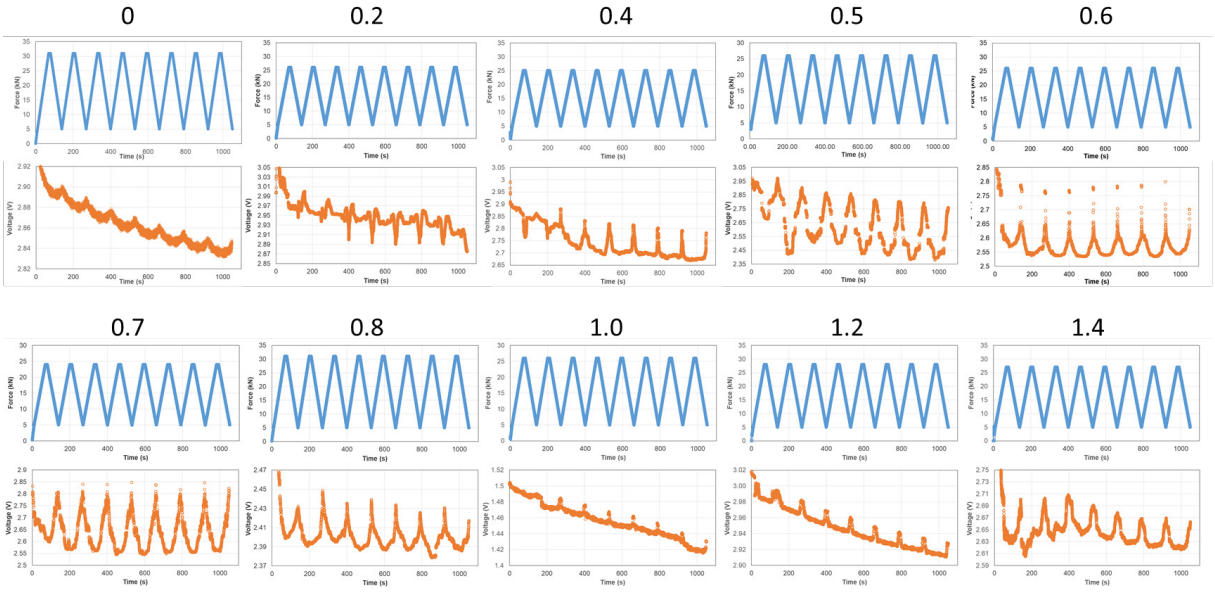

Figure 8. Load-voltage curves for the concrete specimens containing CT12 rCF during the compression tests.

Table 3. Parameters obtained from the load-voltage curves of concrete specimens with C10/30 and CT12 during the compression tests

rCF Content (%)	C10/30		CT12	
	Voltage drop (V)	$\Delta V_{peak-peak}$ (V)	Voltage drop (V)	$\Delta V_{peak-peak}$ (V)
0	−0.09	0.005	−0.09	0.005
0.2	−0.89	0.02	−0.20	0.04
0.4	−0.66	0.11	−0.21	0.10
0.5	−0.35	0.38	−0.22	0.17
0.6	−0.06	0.50	−0.30	0.24
0.7	−0.13	0.15	−0.20	0.27
0.8	−0.32	0.57	−0.16	0.04
1	−0.37	0.41	−0.07	0.009
1.2	−0.09	0.21	−0.09	0.01
1.4	−0.16	0.12	−0.05	0.05

One of the parameters affected by the type of rCF used is the voltage drop measured during the piezo-resistive tests, as shown in Figure 9. The voltage drop is related to the presence of the polarisation phenomenon because of the movement of electrical charges during the test. The polarisation phenomenon usually appears in cementitious materials when they are subjected to an electrical field. Wen et al. have already shown that electrical polarisation diminishes when carbon fibres are incorporated into cementitious matrices [37]. Samples incorporated with C10/30 fibres present very large voltage drops for low fibre contents, and the voltage drop diminishes with an increase in the rCF content. The voltage drop stabilises at approximately −0.1 to 0.2 V. A further increase in the voltage drop in C10/30 samples may be related to the presence of fibre bunches [28]. Samples incorporated with CT12 fibres present a voltage drop

that almost shows no variation with the rCF content. For rCF contents below the percolation threshold value (~0.6% vol.), the voltage drop of CT12 specimens is lower than that of C10/30 samples.

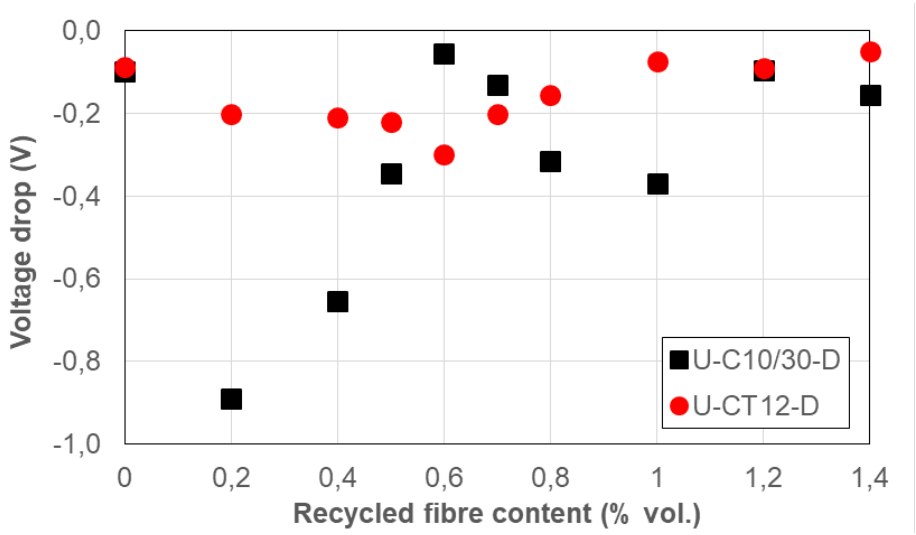

Figure 9. Voltage drop measured during the piezo-resistive tests.

The second parameter influenced by the type and content of rCF is the amplitude of the voltage variation ($\Delta V_{peak\text{-}peak}$). The variation of $\Delta V_{peak\text{-}peak}$ with the rCF content is very similar for concrete samples with both rCF types, C10/30 and CT12, as shown in Figure 10, where three different zones can be identified. In zone I, for low rCF contents (below 0.2% vol.), the $\Delta V_{peak\text{-}peak}$ values are very similar to that observed for the reference sample without rCF. Further increase in the rCF content results in a linear increase in $\Delta V_{peak\text{-}peak}$ up to the percolation threshold value. The slope of the linear variation in zone II is different for C10/30 and CT12 fibres, with the corresponding slopes being 1.02 and 0.49, respectively.

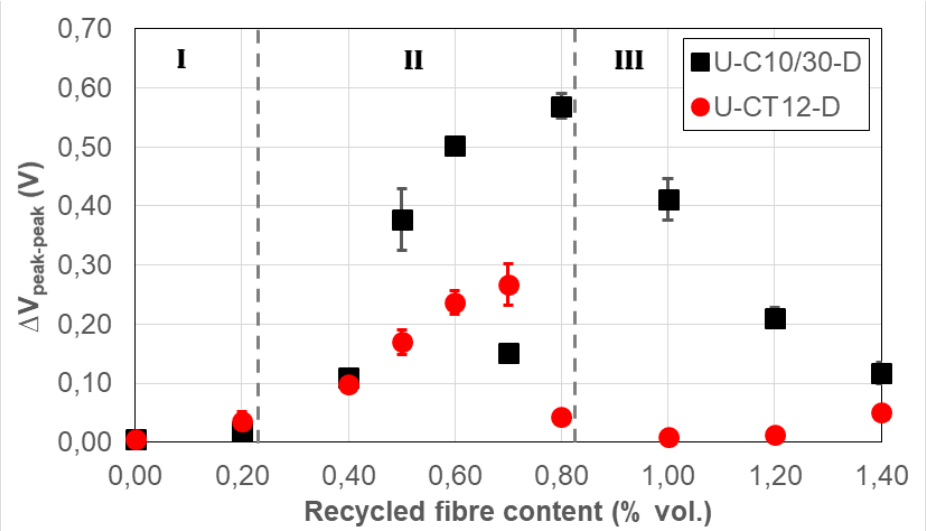

Figure 10. Variation of $\Delta V_{peak\text{-}peak}$ with the rCF content.

The observed behaviour can be explained considering the number of fibres per unit volume, *N*. For rCF contents below 0.4%, the differences in the numbers of fibres per unit volume of CT12 and C10/30 fibres are small, and thus low differences in is expected in the fibre dispersion. However, as the rCF content increases, so does the difference in *N*. Lastly, in zone III, $\Delta V_{peak\text{-}peak}$ diminishes with the fibre content because of the formation of fibre bunches in the cementitious matrix, although the variation is clearly influenced by the fibre type. The samples incorporated with CT12 fibre display a more drastic reduction in $\Delta V_{peak\text{-}peak}$ for rCF contents above the percolation threshold. Thus, the number of fibres per unit volume seems to play a specific role in the conductivity of the concrete, and thus on the observed piezo-resistive phenomenon.

However, some differences are observed when $\Delta V_{peak\text{-}peak}$ is analysed considering the conductivity of the samples (see Figure 11). Considering the hypothesis presented, $\Delta V_{peak\text{-}peak}$ could be expected to increase with the conductivity of the specimens up to a maximum value related to the percolation threshold. The samples incorporated with C10/30 fibres agree with this hypothesis at both 50 Hz and 190 kHz, with some outlier values (clearly identified in

Figure 11 by shaded areas), which will be analysed further. However, samples incorporated with CT12 fibres do not agree with this behaviour when analysed at 50 Hz, but they agree when the values of $\Delta V_{peak\text{-}peak}$ are compared for σ_{190kHz}, with some outlier values.

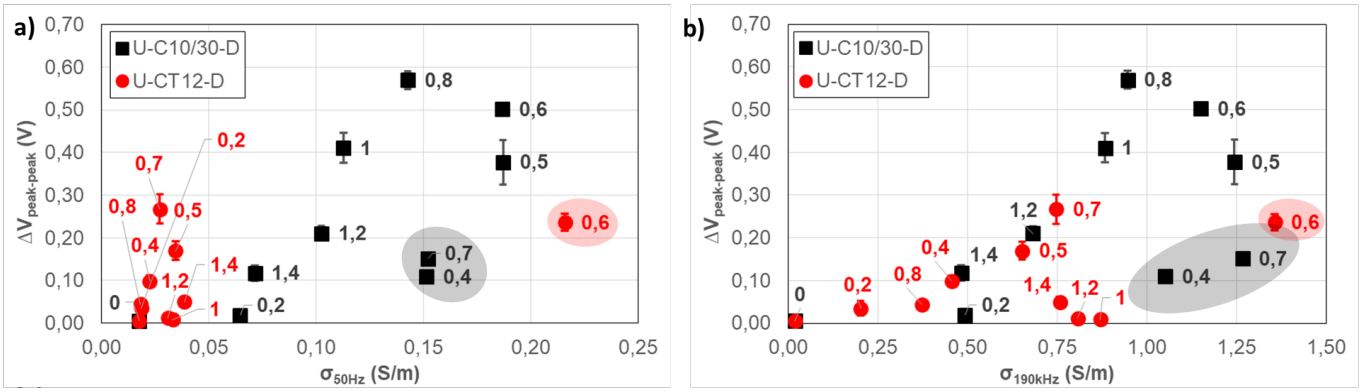

Figure 11. Variation of $\Delta V_{peak\text{-}peak}$ with the conductivity for each rCF type: a) σ_{50Hz}, and b) σ_{190kHz} (outliers identified by shaded areas).

The two values identified as outliers in the $\Delta V_{peak\text{-}peak}$ vs σ curve of the C10/30 samples were also outliers in the $\Delta V_{peak\text{-}peak}$–$V_f$ curve and correspond respectively to the values immediately below and above the percolation threshold (0.4 and 0.7% vol.) Similarly, the outlier in the $\Delta V_{peak\text{-}peak}$–$\sigma$ curve of the C10/30 sample corresponds to the rCF content at the percolation threshold (0.6% vol.). However, the trends observed in the $\Delta V_{peak\text{-}peak}$–$\sigma$ (Figure 11) curves do not correlate completely with the σ–V_f curves (Figure 5).

4. DISCUSSION

Several researchers have proposed models to account for the piezo-resistive responses of conductive cementitious materials. The first studies on this topic were presented by Sun et al. [38] and Wen & Chung [5]. More recently, García-Macías et al. [36] presented a very detailed review on the available models and proposed a new three-dimensional mixed micromechanics-FEM modelling of piezo-resistive CNT smart concrete. Sun et al. [38] described the observation

379 of piezo-resistive effects in plain cementitious materials and explained it in terms of a solid-
380 liquid interface double-layer model. In this situation, when a compressive force is applied, the
381 ions in the double-layer are transported to the cement pore solution because of the interface
382 shear stress. Thus, charges accumulate and a streaming potential difference arises. The load–
383 voltage curve of the reference samples (Figure 6) presents two different phenomena during
384 loading and unloading. During the loading of the sample, the voltage decreases because of a
385 leakage of charges through the conductive paths of the cementitious matrix and the flow of the
386 cement pore solution. During unloading, a part of the solution refills the vacated pores and the
387 voltage is increased. When the rCFs are incorporated into the cementitious matrix, the
388 mechanism is mostly similar because of the cementitious paste that coats the carbon fibres. Two
389 adjacent carbon fibres will always be surrounded by cementitious paste, but the thickness of
390 this interface reduces as the rCF content is increased.
391
392 Thus, the incorporation of rCF does not alter the main mechanism of piezo-resistivity but
393 amplifies the effect by increasing the signal-to-noise ratio. The signal-to-noise ratio, *SNR*, (in
394 dB) is estimated by Eq. 8, as the ratio of the value of a given parameter (σ_{50Hz}, σ_{190kHz}, or $\Delta V_{peak-peak}$)
395 for a concrete sample with a given rCF content to that of the same parameter for the plain
396 concrete sample:

397 $$SNR = 10 \cdot log\left(P_{signal} / P_{noise}\right) \quad \text{(Eq. 8)}$$

398 The influence of the rCF content on the SNR is presented in Figure 12, where two different
399 behaviours can be identified. First, the SNR of σ_{50Hz} and σ_{190kHz} presents a slight increase for
400 rCF contents below the percolation threshold and stabilizes for further increases in the rCF. The
401 average SNR values of σ_{50Hz} and σ_{190kHz} differ significantly for a given fibre type, as shown in
402 Table 4. Moreover, the average SNR values σ_{50Hz} also differ significantly for C10/30 and CT12
403 fibres, however, on the contrary, the SNR values of σ_{190kHz} are very similar. The conductivity

measurements for frequencies below the capacitance threshold (50 Hz) are controlled by the fibre-matrix interface, and thus by the dispersion of the carbon fibres.

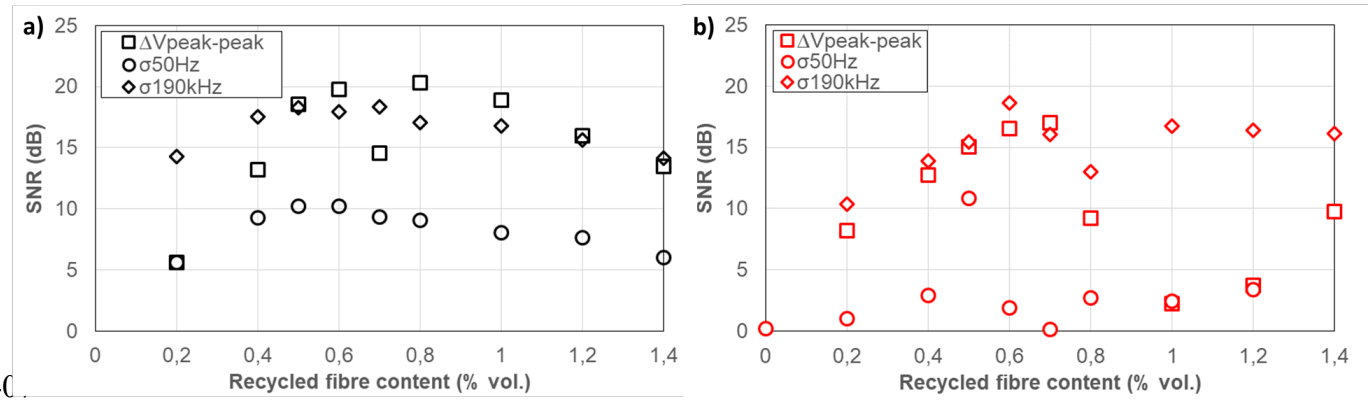

Figure 12. Variation of the SNR of σ_{50Hz}, σ_{190kHz}, and $\Delta V_{peak\text{-}peak}$ for a) U-C10/30-D specimens, and b) U-CT12-D specimens

As discussed previously, the specimens incorporated with CT12 fibres in our study are more likely to present fibre bunches than the ones incorporated with C10/30 fibres, because of the larger number of fibres per unit volume of the former. Therefore, the SNR of σ_{50Hz} reflects the influence of the fibre-matrix interface. However, for frequency values above the capacitance threshold (190 kHz), the conductivity values are mainly influenced by the electronic conduction and the effects of the fibre-matrix interface are reduced. Thus, the SNR of σ_{190kHz} is very similar for both fibre types. The variation in the SNR of $\Delta V_{peak\text{-}peak}$ with the rCF content presents a mixed behaviour between σ_{50Hz} and σ_{190kHz}. For values below the percolation threshold, the SNR values of $\Delta V_{peak\text{-}peak}$ are similar to those of σ_{50Hz}. This behaviour is observed in the samples incorporated with both C10/30 and CT12 fibres. For rCF contents above the percolation threshold, the SNR of $\Delta V_{peak\text{-}peak}$ varies depending on the fibre type: for the C10/30 samples, the SNR almost shows no variation with increasing rCF content, whereas for the CT12 specimens, there is a strong decrease in the SNR followed by an increase for larger rCF

contents. This mixed behaviour may be attributed to a mixed control of the piezo-resistive phenomena in these samples. For rCF contents below the percolation threshold, the main controlling factor is the fibre-matrix interface, whereas for larger rCF contents, the controlling factor varies between the electronic transfer mechanism and the fibre-matrix interface, depending on the characteristics of the fibre dispersion in the cementitious matrix.

Table 4. Average values of SNR for different parameters and rCF types

SNR (dB)	**Fibre type**	
	C10/30	**CT12**
σ_{50Hz}	8.4	2.8
σ_{190kHz}	16.7	15.2
$\Delta V_{peak\text{-}peak}$	15.6	10.5

The observed behaviour is in agreement with previous observations by Sun et al. [39], which were more recently confirmed by Baeza et al. [40], who proposed a constitutive model for the electrical behaviour of carbon fibre-reinforced composites. This model includes four possible conductive mechanisms: 1) ionic conductivity, 2) conductivity due to electronically conductive fibres in the cement matrix and conductive holes, 3) conductivity due to electronically conductive paths between the fibres and the continuous conductive holes, and 4) conductivity due to electronically conductive fibres passing through the conductive network past the conductive hole. For a sample with low carbon fibre content, the main conductive mechanisms are 1) and 2). As the fibre content increases, electrical conduction occurs mainly via mechanisms (2) and (3). When the fibre content is increased above the percolation threshold, mechanism 4) becomes the main pathway. Therefore, the piezo-resistive phenomena shown in Figure 6 and Figure 8 reflect both the influence of the fibre-matrix interface and the electronic transfer mechanism. For low rCF contents, the thickness of the fibre-matrix interface is large and so is the distance between the carbon fibres. Thus, for low rCF contents the fibre-matrix

446 interface in the cementitious matrix will control the piezo-resistive response of the composite.
447 As the rCF content is increased up to the percolation threshold, the thickness of the cementitious
448 matrix surrounding the fibres reduces, and thus the electronic transfer mechanism becomes
449 dominant in the piezo-resistive phenomenon. For rCF contents above the percolation threshold,
450 the presence of fibre bunches and the effect of the fibre waviness will determine the observed
451 behaviour, and thus the fibre-matrix interface increasingly influence the piezo-resistive
452 behaviour.
453

454 **5. CONCLUSIONS**

455 The piezo-resistive phenomenon observed in cementitious materials is inherent to their porous
456 structure and the enclosed aqueous solution. The piezo-resistive effect in these materials could
457 be increased by incorporating carbon fibres. In this article, we demonstrated that rCFs can also
458 be incorporated in cementitious composites to increase their piezo-resistive responses.
459 Furthermore, we showed that the main parameters that control the electrical behaviour of carbon
460 fibre-reinforced cementitious composites (fibre dispersion and fibre waviness) also determine
461 the piezo-resistive responses of our cement composites. For rCF contents below the percolation
462 threshold, the piezo-resistive response is mainly controlled by the thickness of the cementitious
463 paste surrounding the rCF, and thus small piezo-resistive response was obtained. When the rCF
464 was increased, the electronic transfer mechanism started to control the electrical behaviour, and
465 thus the piezo-resistive response increased. However, for rCF contents above the percolation
466 threshold, the presence of fibre bunches and the waviness of the carbon fibres determine the
467 main parameter that controls the electrical behaviour: (i) the fibre-matrix interface and thus the
468 ionic conductivity or (ii) the electronic conduction. The results presented in this paper open new
469 possibilities for the development of smart cementitious materials that can be introduced into
470 civil engineering structures. The use of recycled carbon fibres and of fabrication procedures

similar to those used by the civil engineering industry allow the development of cementitious composites with properties that are equivalent to those of materials fabricated with expensive carbonaceous materials or using sophisticated fabrication and dispersion protocols.

6. Acknowledgements

The authors acknowledge the financial support provided by the Spanish Ministry of Economy and Competitiveness through the Torres Quevedo Program (postdoctoral fellowships, PTQ-14-07072 and PTQ-15-07562), as well as the support from the Catalan Government through the Industrial Doctorate program, DI-2015-013. The authors also thank the company, Escofet 1886 for their collaboration and support throughout the entire project.

7. References

[1] A. Barrias, J. Casas, and S. Villalba, "A Review of Distributed Optical Fiber Sensors for Civil Engineering Applications," *Sensors*, vol. 16, no. 5, p. 748, May 2016.

[2] D. Zonta, H. Wu, M. Pozzi, P. Zanon, M. Ceriotti, L. Mottola, G. P. Picco, A. L. Murphy, S. Guna, and M. Corrà, "Wireless sensor networks for permanent health monitoring of historic buildings," *Smart Struct. Syst.*, vol. 6, no. 5–6, pp. 595–618, Jul. 2010.

[3] H. Ceylan, "Use of smart sensor systems for health monitoring of the transportation infrastructure system," in *3rd International Conference on Transportation Infrastructure*, 2014.

[4] P.-W. Chen and D. D. L. Chung, "Carbon fiber reinforced concrete for smart structures capable of non-destructive flaw detection," *Smart Mater. Struct.*, vol. 2, no. 1, pp. 22–30, 1993.

[5] S. Wen and D. D. L. Chung, "Model of piezoresistivity in carbon fiber cement," *Cem.*

Concr. Res., vol. 36, no. 10, pp. 1879–1885, 2006.

[6] M. Taya, W. J. Kim, and K. Ono, "Piezoresistivity of a short fiber/elastomer matrix composite," *Mech. Mater.*, vol. 28, no. 1–4, pp. 53–59, Jul. 1998.

[7] P. W. Chen and D. D. L. Chung, "Concrete as a new strain/stress sensor," *Compos. Part B Eng.*, vol. 27, no. 1, pp. 11–23, 1996.

[8] Z. Q. Shi and D. D. L. Chung, "Carbon fiber-reinforced concrete for traffic monitoring and weighing in motion," *Cem. Concr. Res.*, vol. 29, no. 3, pp. 435–439, 1999.

[9] D. D. L. Chung, "Cement-matrix composites for smart structures," *Smart Materials and Structures*, vol. 9, no. 4. pp. 389–401, 2000.

[10] D. D. L. Chung, "Cement reinforced with short carbon fibers: A multifunctional material," *Compos. Part B Eng.*, vol. 31, no. 6–7, pp. 511–526, 2000.

[11] F. J. Baeza, O. Galao, E. Zornoza, and P. Garcés, "Multifunctional cement composites strain and damage sensors applied on reinforced concrete (RC) structural elements," *Materials (Basel).*, vol. 6, no. 3, pp. 841–855, Mar. 2013.

[12] F. J. Baeza, E. Zornoza, L. G. Andión, S. Ivorra, and P. Garcés, "Variables affecting strain sensing function in cementitious composites with carbon fibers," *Comput. Concr.*, vol. 8, no. 2, pp. 229–241, Apr. 2011.

[13] Q. Liu, Q. Xu, Q. Yu, R. Gao, and T. Tong, "Experimental investigation on mechanical and piezoresistive properties of cementitious materials containing graphene and graphene oxide nanoplatelets," *Constr. Build. Mater.*, vol. 127, pp. 565–576, 2016.

[14] O. Galao, F. Baeza, E. Zornoza, and P. Garcés, "Carbon Nanofiber Cement Sensors to Detect Strain and Damage of Concrete Specimens Under Compression," *Nanomaterials*, vol. 7, no. 12, p. 413, 2017.

[15] M. S. Konsta-Gdoutos and C. A. Aza, "Self sensing carbon nanotube (CNT) and nanofiber (CNF) cementitious composites for real time damage assessment in smart

structures," *Cem. Concr. Compos.*, vol. 53, pp. 162–169, Oct. 2014.

[16] L. Coppola, A. Buoso, and F. Corazza, "Electrical Properties of Carbon Nanotubes Cement Composites for Monitoring Stress Conditions in Concrete Structures," *Appl. Mech. Mater.*, vol. 82, pp. 118–123, Jul. 2011.

[17] B. Han, X. Yu, K. Zhang, E. Kwon, and J. Ou, "Sensing properties of CNT-filled cement-based stress sensors," *J. Civ. Struct. Heal. Monit.*, vol. 1, no. 1–2, pp. 17–24, Jun. 2011.

[18] S. Dong, B. Han, J. Ou, Z. Li, L. Han, and X. Yu, "Electrically conductive behaviors and mechanisms of short-cut super-fine stainless wire reinforced reactive powder concrete," *Cem. Concr. Compos.*, vol. 72, pp. 48–65, 2016.

[19] Y. Ding, Z. Han, Y. Zhang, and J. B. Aguiar, "Concrete with triphasic conductive materials for self-monitoring of cracking development subjected to flexure," *Compos. Struct.*, vol. 138, pp. 184–191, 2016.

[20] Y. Ding, Y. Huang, Y. Zhang, S. Jalali, and J. B. Aguiar, "Self-monitoring of freeze-thaw damage using triphasic electric conductive concrete," *Constr. Build. Mater.*, vol. 101, pp. 440–446, 2015.

[21] Y. Ding, Z. Chen, Z. Han, Y. Zhang, and F. Pacheco-Torgal, "Nano-carbon black and carbon fiber as conductive materials for the diagnosing of the damage of concrete beam," *Constr. Build. Mater.*, vol. 43, pp. 233–241, 2013.

[22] K. J. Loh and J. Gonzalez, "Cementitious composites engineered with embedded carbon nanotube thin films for enhanced sensing performance," in *Journal of Physics: Conference Series*, 2015, vol. 628, no. 1, p. 12042.

[23] B. Han, S. Ding, and X. Yu, *Intrinsic self-sensing concrete and structures: A review*, vol. 59. Elsevier Ltd, 2015, pp. 110–128.

[24] B. Han, X. Yu, and E. Kwon, "A self-sensing carbon nanotube/cement composite for

546 traffic monitoring," *Nanotechnology*, vol. 20, no. 44, p. 445501, 2009.
547 [25] B. Han, K. Zhang, T. Burnham, E. Kwon, and X. Yu, "Integration and road tests of a
548 self-sensing CNT concrete pavement system for traffic detection," *Smart Mater.*
549 *Struct.*, vol. 22, no. 1, p. 015020, Jan. 2013.
550 [26] S. Pimenta and S. T. Pinho, "Recycling carbon fibre reinforced polymers for structural
551 applications: Technology review and market outlook," *Waste Manag.*, vol. 31, no. 2,
552 pp. 378–392, Feb. 2011.
553 [27] S. J. Pickering, "Recycling technologies for thermoset composite materials — current
554 status," *Compos. Part A Appl. Sci. Manuf.*, vol. 37, pp. 1206–1215, 2006.
555 [28] G. Faneca, I. Segura, J. M. Torrents, and A. Aguado, "Development of conductive
556 cementitious materials using recycled carbon fibres," *Cem. Concr. Compos.*, vol. 92,
557 pp. 135–144, 2018.
558 [29] R. Narayanan and I. Y. S. Darwish, "Use of Steel Fibers as Shear Reinforcement,"
559 *Struct. J.*, vol. 84, no. 3, pp. 216–227, 1987.
560 [30] AENOR, "UNE-EN 196-1:2005 Methods of testing cement. Part I: Determination of
561 strength." 2005.
562 [31] AENOR, "UNE-EN 1015-3:2000 Methods of test for mortar for masonry.
563 Determination of consistence of fresh mortar (by flow table)." 2000.
564 [32] E. Gersing, "Measurement of electrical impedance in organs measuring equipment for
565 research and clinical applications," *Biomed. Tech.*, vol. 36, pp. 6–11, 1991.
566 [33] S. Wen and D. D. L. Chung, "The role of electronic and ionic conduction in the
567 electrical conductivity of carbon fiber reinforced cement," *Carbon N. Y.*, vol. 44, no.
568 11, pp. 2130–2138, 2006.
569 [34] S. Wen and D. D. L. Chung, "Double percolation in the electrical conduction in carbon
570 fiber reinforced cement-based materials," *Carbon N. Y.*, vol. 45, no. 2, pp. 263–267,

2007.

[35] T. O. Mason, M. A. Campo, A. D. Hixson, and L. Y. Woo, “Impedance spectroscopy of fiber-reinforced cement composites,” *Cem. Concr. Compos.*, vol. 24, no. 5, pp. 457–465, 2002.

[36] E. García-Macías, A. D. Alessandro, and R. Castro-triguero, “Micromechanics modeling of the electrical conductivity of carbon nanotube cement-matrix composites,” *Composite*, vol. 108, pp. 451–469, 2017.

[37] S. Wen and D. D. L. Chung, “Electric polarization in carbon fiber-reinforced cement,” *Cem. Concr. Res.*, vol. 31, no. 1, pp. 141–147, 2001.

[38] M. Sun, Q. Liu, Z. Li, and Y. Hu, “A study of piezoelectric properties of carbon fiber reinforced concrete and plain cement paste during dynamic loading,” *Cem. Concr. Res.*, vol. 30, no. 10, pp. 1593–1595, Oct. 2000.

[39] M. Sun, Z. Li, Q. Mao, and D. Shen, “Study on the Hole Conduction Phenomenon in Carbon Fiber-Reinforced Concrete,” *Cem. Concr. Res.*, vol. 28, no. 4, pp. 549–554, Apr. 1998.

[40] F. J. Baeza, O. Galao, I. J. Vegas, M. Cano, and P. Garcés, “Influence of recycled slag aggregates on the conductivity and strain sensing capacity of carbon fiber reinforced cement mortars,” *Constr. Build. Mater.*, vol. 184, pp. 311–319, Sep. 2018.